A 3D distance-weighted Wiener filter for Poisson noise reduction in sinogram space for SPECT imaging

Hongbing Lu*, Jui-Hsi Cheng, Guoping Han, Lihong Li, and Zhengrong Liang
Department of Radiology, State University of New York, Stony Brook, NY 11794, USA

ABSTRACT

A three-dimensional (3D) distance-weighted Wiener filtering, which takes the characteristics of Poisson noise into account as well as the frequency-distance relationship of projection data, is described and evaluated. The task of spatial filtering on Poisson noise can be greatly simplified without the estimation of noise-power spectrum by first applying the Anscombe transformation to the projection data, which converts Poisson distributed noise into Gaussian distributed one with constant variance. By extending the stationary-phase condition and frequency-distance relationship (derived from the noise-free 2D sinogram) into 3D situation, we obtain a weighting function in frequency domain which is only dependent on the distance of an interested point source from the object center. Since the Anscombe transformation only changes the distribution of projection data, not the pixel location, a distance-variant weighting window for the Anscombe transformed data is derived and incorporated into the Wiener filter. Considering the regions with higher signal-to-noise ratio (SNR) receive greater weight in the estimation of signal-power spectrum, the proposed filter optimizes the data used to estimate the power spectrum of observed data and thus produces a better spatial resolution. Simulation and experimental results show improved noise reduction, especially in the peripheral regions, as compared with conventional filtering methods.

Keywords: Poisson noise, SPECT imaging, Anscombe transformation, distance-weighted, 3D Wiener filter.

1. INTRODUCTION

For brain single-photon emission computed tomography (SPECT), an exact inversion of noise-free, attenuated Radon transform in a uniform attenuating medium (i.e., exponential Radon transform) has been reported [1,2]. The usefulness of the inversion depends on the success of smoothing the Poisson noise, which varies depending on the intensity at each voxel (i.e., signal dependence) and renders a very challenging task. The Poisson noise probably is the major factor that influences the quantitative capability of SPECT due to the low-count density limitation. Conventional techniques for noise reduction use low-pass filters to smooth each projection image separately, ignoring the signal-dependent nature of Poisson noise and the angular correlation among projections. Therefore, the noise reduction is achieved at the cost of spatial resolution [3]. Theoretically, almost all the conventional techniques assume that the noise is additive white Gaussian distributed, which might be a reasonable approximation in high-count situation, but is not justified in low-count SPECT imaging. Treatment of signal-dependent noise has been attempted by several authors [4-7]. King et al [4] implemented the Metz filter by adjusting the filter parameters to consider the total photon count in each image, but with little progress to make the processing adaptive to the noise spatial-dependence or to take the advantage of the noise statistic property. La Riviere et al [5] proposed a sinogram smoothing approach, in which a non-parametric regression using a roughness-penalized Poisson likelihood objective function is employed. The approach was found to have desirable uniform and isotropic resolution property and yield resolution-noise tradeoffs superior to those of shift-invariant filtering methods. Although the simulation results are promising, the iterative process demands intensive computational effort and the free-adjustable smoothing parameters remain undetermined. Chan et al [6] and Kuan et al [7] achieved empirically some degree success in the specific tasks.

As an optimal filter which achieves *Linear Minimum Mean-Square Error* (LMMSE), Wiener filter removes noise in a stochastic sense and has been applied successfully in various situation of de-noising [3,8,9]. However, its assumption that the signal is a stationary random process is not valid near the edges and boundaries in the image. It has been recognized that the Wiener filter outperforms other filters in the areas where stationary assumption is reasonably satisfied, while in areas where spatial sharp edges are present, the "averaging" of nearby pixels could cause artifacts and blur the filtered sequence [3]. To avoid these limitations while maintaining good noise suppression, a weighting window can be incorporated into the filter with spatially-varying or frequency adaptive weights. The weighting given to the areas with low signal-to-noise ratio (SNR) should be lessened, while that to the areas with high SNR should be enhanced. This weighting will adjust adequately the amount of spatial smoothing applied to these areas. Another requirement for the use of Wiener filter is the knowledge of the

* Correspondence: hblu@clio.rad.sunysb.edu; phone 1 631 444-2736; fax 1 631 444-6450; http://www.sunysb.edu/micl/; State University of New York, Stony Brook, NY, USA 11794

Medical Imaging 2001: Physics of Medical Imaging, Larry E. Antonuk, Martin J. Yaffe, Editors,
Proceedings of SPIE Vol. 4320 (2001) © 2001 SPIE · 1605-7422/01/$15.00

signal and noise covariance matrix of the data. In general, this is not available. Although the method for estimating the signal covariance is apparent, the method for estimating noise covariance is not, especially in cases of noisy SPECT data.

In our previous studies, a 2D Wiener filter with butterfly window, which includes *a priori* information to treat Poisson noise in the sinogram space in the frequency domain, has been investigated [10,11]. In this paper, we extend the 2D filtering to 3D cases. The Anscombe transformation is first applied to transform Poisson distributed noise into Guassian distributed one, which greatly simplified the estimation of noise-power spectrum. Then we extend the stationary phase condition and frequency-distance relation, derived from the frequency distribution of noise-free sinogram, into 3D situation. By converting the distance-weighted algorithm proposed by Nowak et al [12] in spatial domain into frequency domain, we propose a distance-weighted 3D Wiener filter to achieve an adaptive filtering, for preserving edge information while reducing the noise.

2. METHODS

2.1. Noise model

It is well known that the observed SPECT data $\boldsymbol{y}$ are Poisson-distributed with means given by $\boldsymbol{Hf}$ [6], i.e.,

$$\boldsymbol{y} \sim Poisson(\boldsymbol{Hf}) \tag{1}$$

in which $\boldsymbol{y}$ is a $M\times 1$ vector obtained by lexicographic ordering of the observed SPECT projection data, $\boldsymbol{f}$ is a $N\times 1$ vector obtained by lexicographic ordering of the discrete representation of the true image intensity, and $\boldsymbol{H}$ is a $M\times N$ system matrix representing the action of the response functions applied to the projecting process from source to observed data.

With this model, the goal in tomographic reconstruction can be expressed as to estimate the discrete activity distribution $\boldsymbol{f}$ from the measured $\boldsymbol{y}$ at a finite number of angles and bins. The noise suppression problem then can be viewed as follows. For a given single realization of a jointly independent Poisson distributed $\boldsymbol{y}$, how can we estimate its mean $\boldsymbol{p}$, ($\boldsymbol{p=Hf}$)? Given the mean $\boldsymbol{p}$, the source $\boldsymbol{f}$ can be reconstructed by the inversion of the exponential Radon transform. In this paper, we will focus on the statistical problem of fitting smooth curves to the noisy measurement $\boldsymbol{y}$ in order to estimate $\boldsymbol{p}$, instead of estimate $\boldsymbol{f}$ directly.

For MMSE filtering, it's more convenient to express the noise as an additive term

$$\boldsymbol{y} = \boldsymbol{p} + \boldsymbol{n} \tag{2}$$

where the mean of the noise $\boldsymbol{n}$ equals to $\boldsymbol{0}$ and the variance equals to $E(\boldsymbol{p})$, depending on the signal itself [6,11].

For given observed data $y(s, z, \theta)$ at detection bin (s,z) and projection angle θ, Eq.(2) becomes $y(s, z,\theta)=p(s, z,\theta)+n(s, z,\theta)$, where $p(s, z,\theta)$ is the signal to be estimated and $n(s, z,\theta)$ is the noise. Assume that the noise is uncorrelated with the signal and also with each other, and further assume that the projection data are spatially stationary, the Wiener filter in the frequency domain then has the form [8,11]

$$\begin{aligned} H(\omega_s,\omega_z,k_\theta) &= \frac{S_{yp}(\omega_s,\omega_z,k_\theta)}{S_{yy}(\omega_s,\omega_z,k_\theta)} \\ &= \frac{S_{yy}(\omega_s,\omega_z,k_\theta) - S_{nn}(\omega_s,\omega_z,k_\theta)}{S_{yy}(\omega_s,\omega_z,k_\theta)} \end{aligned} \tag{3}$$

where S_{yp}, S_{yy}, and S_{nn} are the cross-power spectrum of y and p, and the power spectra of y and n, respectively. The implementation of the Wiener filter is thus simplified to determine S_{yy} and S_{nn}.

Considering the signal-dependent property of Poisson noise, the implementation of Wiener filter for SPECT modality seems very challenging, because any error resulting from the estimation of noise variance, which is unknown and needs to be estimated from noisy data, will degrade the accuracy of filtering. Traditional estimation of noise variance using sampled data mean is not satisfactory, since it ignores the signal dependent property. Instead, we found that an alternative estimation of S_{nn} can be achieved by Anscombe transformation [13].

2.2. Anscombe transformation

Anscombe transform, which was also referred as square-root transform [10,14], was proposed by F. Anscombe in 1948. He proved that if x is Poisson distributed with mean equal to λ, then $y= (x+3/8)^{1/2}$ can be approximated as Gaussian distributed

with its mean equal to $(\lambda+1/8)^{1/2}$ and its variance equal to 0.25 [11]. Here we call this transform as Anscombe because it's quite different from the meanings of square-root transform.

By performing Anscombe transform, the Poisson noise model can be rewritten as

$$\boldsymbol{y'} = \boldsymbol{p'} + \boldsymbol{n'} \tag{4}$$

where *y'*, *p'*, and *n'* denote the $M\times 1$ vectors obtained by lexicographically ordering the observed data, the original projections (to be estimated), and the noise, respectively, after Anscombe transformation. Then n'_j would be a Guassian distributed noise with constant variance *0.25* at pixel *j*. Thus, an accurate Wiener filter can be constructed without estimation of the noise-power spectrum. In our previous work [10], we verified the performance of Anscombe transform by numerical calculation. The results showed good accordance between two distributions. Strictly speaking, the transform from Poisson distribution to Guassian distribution can not be achieved exactly since one is the discrete random process, while the other is continuous random process. The claim that this transform can achieve the goal is only based on the first two orders of statistics. It is noted that the joint independence of $\boldsymbol{y'}$ remains after the transform, and the assumption of spatial stationary for $\boldsymbol{y'}$ is more reasonable after the transform, in addition to the removal of signal dependence of the measured noisy data.

The remaining task of applying Wiener filter in SPECT imaging is the estimation of S_{yy} in Eq.(3). The estimation of the power spectrum of the observed data has been extensively investigated in the past decades [14]. However, none of these techniques were designed specially for SPECT. By analyzing the frequency distribution of the noise-free sinogram and the attenuation effect in the frequency domain, we propose a distance-weighted window to improve the estimation of signal power spectrum, as described in following sections.

2.3. Extension of stationary-phase condition and frequency-distance relation to 3D situation

2.3.1. Stationary-phase Condition

By analyzing the frequency distribution of a noise-free sinogram, we observed that only regions satisfying the following property have significant contribution to the frequency distribution [15],

$$r_p \sin(\phi_p - \theta) = \frac{k_\theta}{\omega_s} \tag{5}$$

which is called as the stationary phase condition. By examining this condition, we further observed that for noise-free case, its frequency distribution is approximately zero if the following description is satisfied [15]

$$\left| \frac{k_\theta}{\omega_s} \right| > r_p \tag{6}$$

where ω_s and k_θ represent Fourier transform (FT) of *s* and θ. The notations r_p and Φ_p stand for the polar coordinates of a point source, while θ means the projection angle.

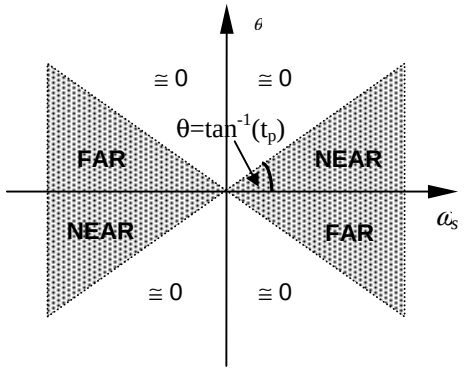

Figure 1. Fourier distribution of noise-free sinogram of source points [15].

By extending the stationary phase condition to 3D situation, we found that the above feature is still preserved for any point $P(\omega_s,\omega_z,k_\theta)$ in 3D frequency domain, where r_p is the maximum vertical distance from the object boundary to the rotation center. Since stationary phase condition depends only on the boundary location of the object, it is also applicable for the

Anscombe transformed projection data. Considering that this frequency-distribution characteristics would not exist for noisy sinogram, we design a window mask which assigns zero to regions satisfying Eq.(5) and assigns 1 to the rest areas (shadow areas) to minimize noise propagation and improve the estimation of signal power spectrum, as shown in Fig.1. It should be noted that when different thresholds are selected to decide the boundary of the object, different window masks are obtained.

2.3.2. Frequency-distance relationship

From the stationary phase condition of Eq.(5), we can directly obtain a remarkable simple form

$$t_p(\theta) = -\frac{k_\theta}{\omega_s} \tag{7}$$

which has been referred to as the "frequency-distance relation" [15], where $t_p(\theta)$ represents the distance from a point (r,θ) within the object to the rotation axis. It means that as θ goes from *0* to 2π, the most significant contribution of an arbitrary point object to the Fourier coefficient occurs at an angle value of θ such that the point has a distance t_p to the rotation axis is $-k_\theta/w_s$ [13]. If only those Fourier coefficients for which $k_\theta/\omega_s > 0$ were selected, then those data with contributions from points near the detector would be used for the restoration, since those data carry better resolution and sensitivity information. For data collected within a full 360° range of views, a particular point source in the object will have negative t_p (with a shorter distance to the detector than the rotation center) for a subinterval of 180° within the full range of views. The data collected in this subinterval of 180°(called near field) would be better for accurate reconstruction of that point than the data from the far-field, as shown in Figure 1. To improve the reconstruction resolution and noise reduction, a weighting window should be designed to enhance the near-field components in the power spectrum estimation, and lessen the far-field components. This will enhance SNR and reduce the amount of spatial smoothing applied to the near-field region.

2.4. Design of weighting window

As we discussed above, the design of the weighting window should consider the observation that the contributions of near-field voxels to the projections must be greater than those voxels far away from the detector. The task becomes how to construct the weighting scales. Although some published papers have described several frequency-distribution relationships between the uniform-attenuated and the attenuation-free projection data, all of them can not be directly applied, because after Anscombe transform the original promise of the attenuated data would not be guaranteed anymore [11,15,16].

In the weighted backprojection method proposed by Tanaka [16], a reconstruction index was used to determine the relative weights which is imposed on two conjugate projections to form an image. Tanaka found that the variance of the noise at off-center is strongly affected by the index. The use of a positive index implies that a larger weight is imposed to the front projection than to the rear projection, which is generally preferable as we discussed above, while a negative index would increase the statistical noise at the peripheral area appreciably [16,17]. Unfortunately, the optimal index could not be utilized directly here because the situation is quite different in frequency domain after Anscombe transform. Nowark et al proposed a SPECT reconstruction technique named distance-weighted backprojection, in which the relative amounts of attenuation between opposing views was used to obtain weighting scheme such that the voxel receives greater weights from the closest planar views, as shown in Fig.2 [12].

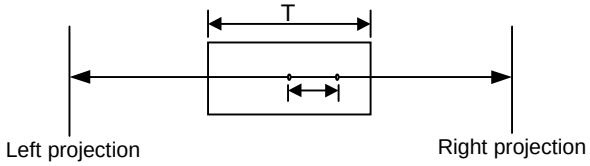

Figure 2. The projecting diagram of a point source P located at a distance *x* from the center of the attenuation medium [12].

In Fig.2, the uniform attenuation medium has a width T, an attenuation coefficient μ_0, and the center C. For any point P located at a distance *x* from the center C, the fraction of the activity received at the right projection, FR, is

$$FR = e^{-\mu_0\left(\frac{T}{2}-x\right)} \tag{8}$$

while the fraction of the activity received at the left projection, FL, is

$$FL = e^{-\mu_0\left(\frac{T}{2}+x\right)} \tag{9}$$

Then the relative amount of original activity received in each projection, WL and WR, can be obtained respectively [12]

$$WL = \frac{FL}{FR + FL} = \frac{1}{1 + e^{2\mu_0 x}}, \tag{10}$$

$$WR = \frac{FR}{FR + FL} = \frac{1}{1 + e^{-2\mu_0 x}}. \tag{11}$$

Notice that these two weighting functions are only dependent on the distance x of the point source from the rotation axis. Both of them are independent of the attenuating medium width, T. Considering that Anscombe transform only changes the activity distribution of projection data, not the voxel location, the relative weighting factors for Anscombe transformed data can be obtained approximately by a similar procedure as described above

$$WL' \cong \frac{1}{1 + e^{\mu_0 x}}, \qquad WR' \cong \frac{1}{1 + e^{-\mu_0 x}}. \tag{12}$$

The difference among Eqs.(10), (11), and (12) results from the square root operation of the Anscombe transform.

From the definition of x and t_p, we find that they are negatively equal. By replacing x with $-t_p$ and substituting frequency-distance relation of Eq.(7) into Eq.(12), we obtain the distanced-weighted window in frequency domain, as shown below

$$W(\omega_s, \omega_z, k_\theta) = \begin{cases} 1 \Big/ 1 + e^{-\mu_0 k_\theta / \omega_s}, & near-field \\ 1 \Big/ 1 + e^{\mu_0 k_\theta / \omega_s}, & far-field \\ 0, & other\ field \end{cases} \tag{13}$$

where the weighting scale is determined to provide greater weight to the regions with higher SNR and resolution to improve the estimation of the signal power spectrum.

2.5. 3D distance-weighted Wiener filter

Incorporating the expressions of weighting window into Eqn.(3), we obtain the final expression for the 3D distance-weighted Wiener filter

$$H(\omega_s, \omega_z, k_\theta) = \frac{S_{yy'}(\omega_s, \omega_z, k_\theta) W((\omega_s, \omega_z, k_\theta) - 0.25}{S_{yy'}(\omega_s, \omega_z, k_\theta) W(\omega_s, \omega_z, k_\theta)} \tag{14}$$

where $S_{yy'}$ is the power spectrum of Anscombe transformed projection data y'.

In summary, the filtering algorithm consists of four steps: Anscombe transform of observed projections; 3D weighted Wiener filtering; normalization of filtered data; and inverse Anscombe transform of the processed data using y'^2-1/8.

3. SIMULATION AND EXPERIMENTAL RESULTS

The proposed method was tested by digital phantom simulations and physical phantom experiments. In the digital simulations, the Hoffman digital brain phantom was used as the emission distribution. The phantom was specified on a 128x128x128 grid. Projections of 128x128 bins were simulated at 128 angles evenly spaced on a circular orbit, using strip integrals with the same width as the bins, which in turn were the same size as the voxels. In the meantime, a circular attenuation map with constant coefficient factor 0.05 was used to simulate the attenuating effect. Scatter and collimator-blurring effect were not considered in the simulations. The simulated projection data were then contaminated by adding Poisson noise. In the experimental work, the Hoffman physical brain phantom was scanned by a triple-head SPECT system with low-energy, high-resolution, parallel-beam collimators. The phantom was injected with 15mCi Tc-99m solution mixed with 1050 ml water. Projection data were sampled on a grid of 128×128 per view over 128 views evenly spanning on a circular orbit. The projection data sets were "smoothed" by different filtering methods for comparison purpose. The smoothed projections were reconstructed by the conventional filtered backprojection (FBP) method (without attenuation compensation to show the noise reduction effect).

3.1. Simulation results

Figure 3 shows the same slice of the reconstructed images and the horizontal profiles drawn from the same slices filtered by different methods in the digital simulation study. The performance of proposed method is compared against that provided by conventional Rectangular filter (no noise reduction), Hanning filter, Shepp-Logan filter, and direct Anscomebe transform + 3D Wiener filter (without the weighting) after FBP reconstruction. The results directly from Rectangular filter are neither qualitatively nor quantitatively acceptable and, therefore, a smoothing filter is required in clinical situation. The results from the commonly used low-pass filters, such as Hanning with cutoff at 0.5 and Shepp-Logan with cutoff at 0.4, demonstrate a trade-off between noise smoothing and resolution preserving. As recognized by many researchers, a significant drawback of these spatially invariant filters is that they treat all of the projection data equally, neglecting the data's inherently statistics, which we are addressing and aiming to improve in this paper. The difference between the reconstructed images using Anscombe transform + 3D Wiener filter with/without the weighting windows seems not significant by visual inspection on the images and the profiles. The reason may be due to the simplified circular phantom in the simulations, where the attenuation is the same for all slices. Experiments on physical phantom showed more difference. This indicated that the proposed method could achieve improvement by the weighting window for object-specific attenuation. Quantitative analysis on the reconstructed images, as presented below, demonstrates a noticeable improvement by the weighting window.

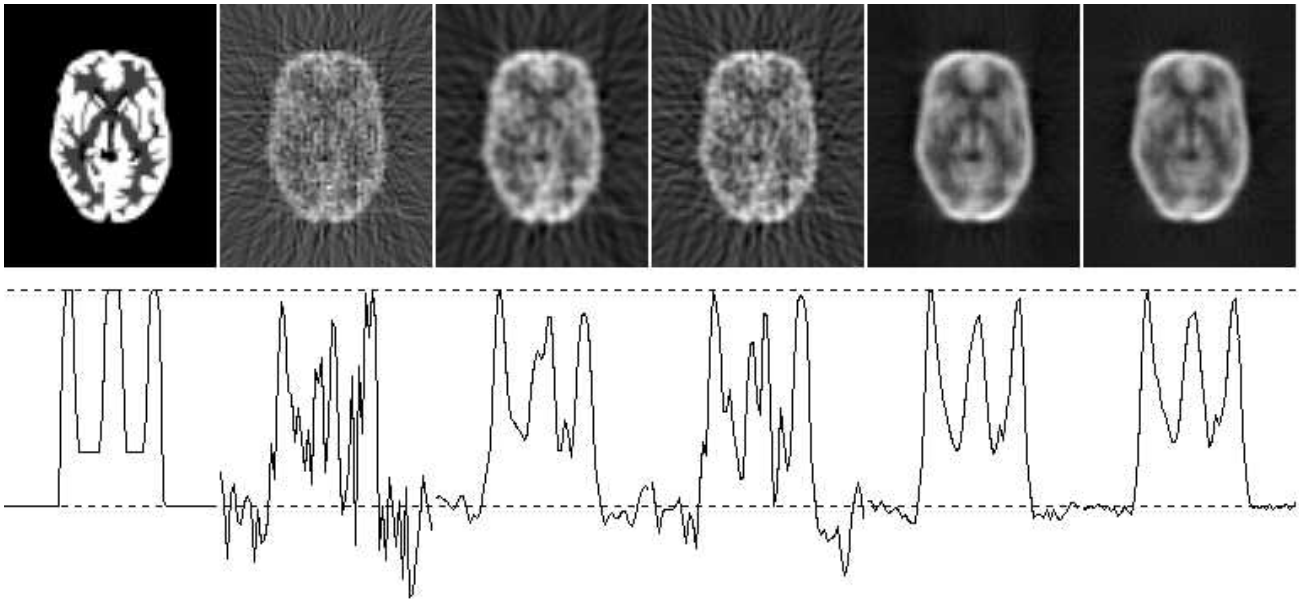

Figure 3. Comparison of the 61st slice of the reconstructed images and the horizontal profiles drawn from that slice, using different filtering methods along the lines indicated. From left to right: phantom, noise-free, noisy data filtered by Shepp-Logan. Hann, direct 3D Wiener filter and proposed method.

3.2. Bias-variance Plot

We evaluated the noise reduction performance of our Wiener filtering method in terms of the statistical bias-variance tradeoff for the entire image, in addition to the subjective quality of visual judgement. The bias and variance of each slice are defined as follow:

$$Bias_i(\%) = 100\frac{1}{M}\sum_{j=1}^{M} | \hat{f}_{i,j} - f_{i,j} | \tag{15}$$

$$Variance_i(\%) = 100\frac{1}{M}\sum_{j=1}^{M} (\hat{f}_{i,j} - f_{i,j})^2, \quad i = 1,2,...,K \tag{16}$$

where $f_{i,j}$ and $f_{i,j}$ represent the activity at pixel j of slice i, reconstructed from noise-free and filtered noisy projection data, respectively. M is the total pixel number of each slice.

The bias-variance plots from 10 different slices are generated to assess the performance of proposed filter against other filtering schemes, such as Hanning filter, Shepp-Logan filter, and the direct 3D Wiener filter without weighting window. To compare the filtering effect on attenuated projection data, two kinds of bias-variance plots are obtained. One comes from the images reconstructed from projections without attenuation effect. The other comes from the images reconstructed from

projections with attenuation effect, as shown in Fig.4. All the reconstructed images were normalized to ensure that the total number of counts in the reconstructed slice was equal to the total number of counts of the same slice in the original Hoffman phantom, so that absolute quantitative analysis could be performed.

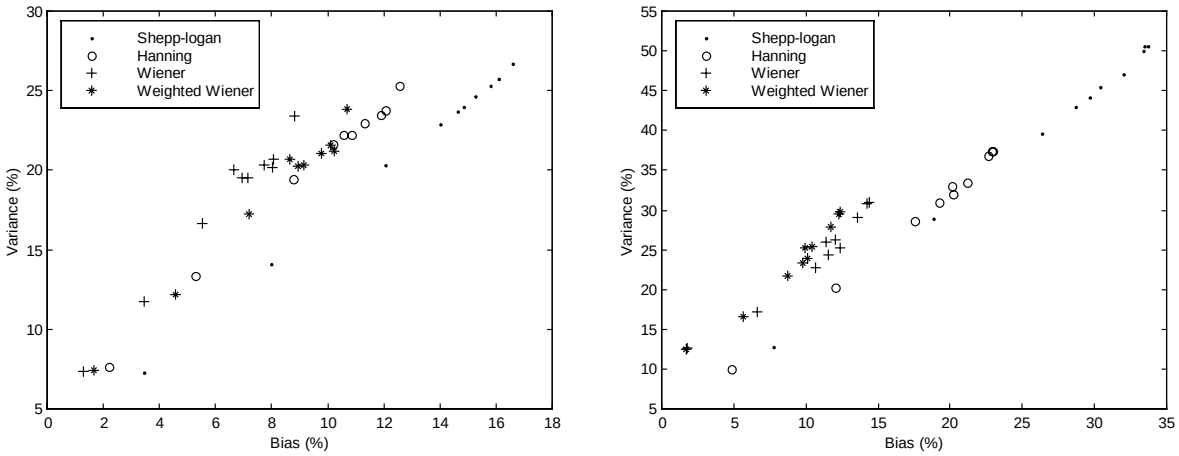

Figure 4. Bias-variance plot for reconstructions filtered with different methods. Left: reconstructed from projections without attenuation effect. Right: reconstructed from projections with attenuation.

From Fig.4, we can see that 3D Wiener filtering with/without weighting outperform the low-pass filters in both situations no matter whether the attenuation effect is simulated. For images reconstructed from projections without attenuation, direct 3D Wiener filter shows better bias-variance trade-off than weighted Wiener filter. However, Weighted Wiener filter outperforms the one without weighting window when attenuation is simulated. That means that the proposed method has a better trade-off between resolution preserving and noise smoothing when applied to attenuated projection data.

3.3. Phantom Experimental Results

The comparison of the proposed method against other filtering approaches using experimental data is shown in Fig.5. We show four slices of reconstructed images for each of the four methods. The reconstructed images filtered by ramp filter (no noise smoothing) and Haning filter (cutoff frequency of 0.5) reveal insufficient noise suppression, while those filtered by direct Anscombe + 3D Wiener filter show a little over-smoothed. The 3D Wiener filter with an appropriate weighting window demonstrates a better noise reduction effect without sacrifice of edge details, especially in the peripheral regions. Comparing the results of Fig.4 and Fig.5, we can observe that our Wiener filter comes with a better noise reduction and better spatial resolution for attenuated projection data.

4. DISCUSSION AND CONCLUSIONS

In this paper, a distanced-weighted 3D Wiener filter derived from frequency distribution of noise-free sinograms has been developed to reduce noise for 360° scanning in SPECT imaging. Unlike the conventional low-pass filters, the design of this filter takes the characteristics of Poisson noise into account as well as frequency-distance relations of projection data. Anscombe transformation is first applied to all projection data, which transform Poisson distributed noise into Guassian distributed with constant variance, enable us to estimate the power spectrum of noise accurately. To ensure the regions with higher SNR receive greater weights in the estimation of signal power spectrum, we first extend the stationary phase condition derived from frequency distribution of noise-free sinograms into 3D situation, and assign zero to weighting window in regions which have no contribution to the frequency distribution. Then by extending frequency-distance relation of sinogram into 3D situation and transforming the spatial distance-weighted algorithm proposed by Nowak et al into frequency domain, a distance-variant weighting window is derived and then incorporated into the filter. Since a variable weighting factor proportional to regional SNR is applied in the estimation of signal power spectrum, the filter is adaptive in preserving edge information while reducing noise. The phantom experiments are very encouraging, by visual judgement, as compared to conventional low-pass filter. Bias-variance analysis also confirms the better resolution-noise trade-off of the proposed method for attenuated projections. Since the spatial resolution of a detector system with parallel-beam collimators generally decreases with increasing distance between the source and collimator and, furthermore, the true-to-scatter ratio decreases with increasing the depth of the source in the object, our proposed method can be very helpful to achieve a higher spatial resolution restoration and a higher true-to-scatter ratio recovery.

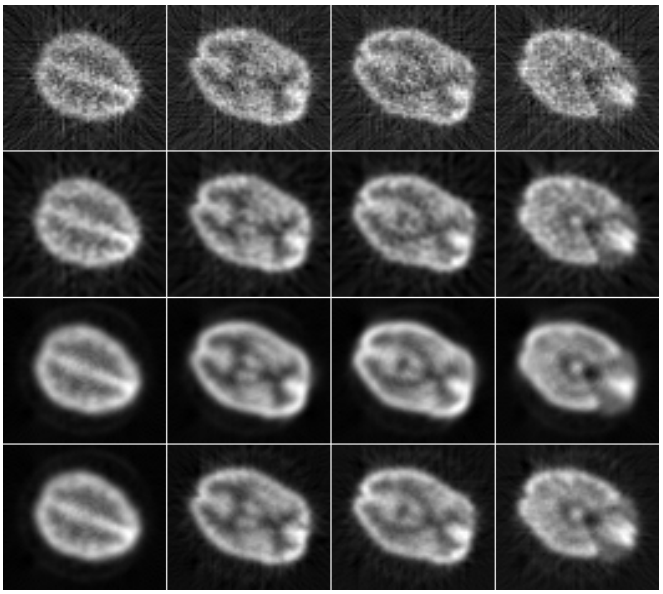

Figure 5. FBP reconstructed transverse slices from experimental data using different filtering approaches. The images from left to right represent transverse slices 57, 67, 70, and 74, respectively. The transverse slices reconstructed from noisy data filtered by Ramp, Hanning, Anscombe transform+3D Wiener filter and proposed method are shown from top to bottom. Scatter, collimator/resolution variation, and attenuation are not compensated.

The stationary requirement for direct implementation of Wiener filter on the observed data is not satisfied in brain SPECT imaging, especially around the edge and boundary of the sinogram. To mitigate the limitation, we optimize the processed data to estimate the power spectrum of the observed data and make the filtering adaptive to achieve a better spatial resolution. This is particular true in the peripheral regions of the reconstructed object. Whereas the proposed method produces a better image quality than conventional filtering methods, it should be noticed that it has no influence on the absolute quantification of the emission uptake. The weighting window is only used to improve the estimation of power spectrum of the signal, not the estimation of activity distribution. However, the proposed distance-weighted algorithm in spatial domain by Nowak et al uses variable weighting factors to the data in such a way that the pixel receives a greater weight from the closest planar views [12], thus the algorithm can influence the absolute quantification of the radiotracer uptake.

Although the power spectrum of Poisson noise can be approximated quite accurately by Anscrombe transformation, the estimation of the power spectrum of observed data $S_{yy}(\omega_s,\omega_z,k_\theta)$ is a complex task, requiring further investigation. We partly addressed this task in this study and will further investigate it in the future.

ACKNOWLEDGEMENTS

This work was partially supported by NIH Grant #HL54166 of the National Heart, Lung and Blood Institute; Grant #NS33853 of the National Institute of Neurological Disorder and Stroke; and the Established Investigator Award of the American Heart Association.

REFERENCES

1. T. Inouye, K. Kose, and A. Hasegava, " Image reconstruction algorithm for SPECT with uniform attenuation", *Phys. Med. Biol.*, **34**, pp.299-304, 1989.
2. X. Pan and C.E. Mets, "Analysis of noise properties of a class of exact methods of inverting the 2-D exponential radon transform," *IEEE Transactions on Medical Imaging*, **14**, pp.659-668, 1995.
3. J.C. Brailean, R.P. Kleihorst, S. Efstratiadis, and et al, "Noise reduction filters for dynamic image sequences: A review," *Proc. IEEE*, **83**, pp.1272-1291, 1995.
4. M.A. King, P.W. Doherty, R.B. Schwinger, and et al, "Fast count-dependent digital filtering of nuclear medicine images: Concise communication", *J. Nuclear Medicine*, **24**, pp.1039-1045, 1988.
5. P.J. La Riviere and Xiaochuan Pan, "Nonparametric regression sinogram smoothing using a roughness-penalized Poisson likelihood objective function", *IEEE Transactions on Medical Imaging*, **19**, pp.773-786, 2000.

6. C.L. Chan, A.K. Katsaggelos, and A.V. Sahakian, "Image sequence filtering in quantum-limited noise with applications to low-dose fluoroscopy," *IEEE Transactions on Medical Imaging*, **12**, pp.610-621, 1992.
7. D.T. Kuan, A.A. Sawchuk, T.C. Strand, and et al, "Adaptive noise smoothing filter for images with signal-dependent noise," *IEEE Trans. Patt. Anal. Mach. Intel.*, **7**, pp.653-665, 1985.
8. Z.H. Cho and J.R. Burger, "Construction, restoration, and enhancement of 2 and 3-dimensional images," *IEEE Transactions on Nuclear Sciences*, **NS-24**, pp.886-892, 1977.
9. E.T. Tsui and T.F. Budinger, "A stochastic filter for transverse section reconstruction," *IEEE Transactions on Nuclear Sciences*, **NS-26**, pp.2687-2690, 1979.
10. J.H. Cheng, Z. Liang, J. Ye, and et al, "Inclusion of a Priori information in frequency space for quantitative SPECT imaging," *1996 IEEE Conference Record of the NSS and MIC*, 1996.
11. J.H. Cheng, *Frequency-domain approaches to quantitative brain SPECT*, Ph.D. Thesis, Dept. of Radiology and Computer Science, State University of New York at Stony Brook, 1997.
12. D.J. Nowark, R.L. Eisner, and W.A. Fajman, "Distance-weighted backprojection: A SPECT reconstruction technique," *Radiology*, **159**, pp.531-536, 1986.
13. F.J. Anscrombe, "The transformation of Poisson, binomial and negative-binomial data," *Biometrics*, **35**, pp.246-254, 1948.
14. F.J. Harris, " On the use of windows for harmonic analysis with the discrete Fourier transform," *Proc. IEEE*, **66**, pp.51-83, 1978.
15. R.M. Lewitt, P.R. Edholm, and W. Xia, "Fourier method for correction of depth-dependent collimator blurring," *Proc. SPIE*, **1092**, pp.232-243, 1989.
16. E. Tanaka, "Quantitative image reconstruction with weighted backprojection for single photon emission computed tomography," *J. Computer Assisted Tomography*, **7**, pp.692-700, 1983.
17. S.H. Manglos, R.J. Jaszczak, and C.E. Floyd, "Weighted backprojection implemented with a non-uniform attenuation map for improved SPECT quantitation," *IEEE Transactions on Nuclear Sciences*, **NS-35**, 1988.